

Received May 3, 2021, accepted June 1, 2021, date of publication June 7, 2021, date of current version June 15, 2021.

Digital Object Identifier 10.1109/ACCESS.2021.3086984

# Application Requirement-Driven Automatic ISP Parameter Tuning for a Rear View Monitoring Camera

YOUN JOO LEE<sup>1</sup>, JAE KYU SUHR<sup>2</sup>, (Member, IEEE),  
AND HO GI JUNG<sup>3</sup>, (Senior Member, IEEE)

<sup>1</sup>Next Generation Unmanned Vehicles Research Center, Sejong University, Seoul 05006, South Korea

<sup>2</sup>School of Intelligent Mechatronics Engineering, Sejong University, Seoul 05006, South Korea

<sup>3</sup>Department of Electronic Engineering, Korea National University of Transportation, Chungju 27469, South Korea

Corresponding author: Ho Gi Jung (hogijung@ut.ac.kr)

This work was supported in part by Hyundai Mobis, in part by the Basic Science Research Program through the National Research Foundation of Korea (NRF) funded by the Ministry of Education under Grant 2020R1A6A1A03038540, and in part by the Ministry of Science and ICT (MSIT), South Korea, through the Grand Information Technology Research Center Support Program supervised by the Institute for Information & Communications Technology Planning & Evaluation (IITP) under Grant IITP-2021-2020-0-01462.

**ABSTRACT** An image signal processor (ISP) is a dedicated processor that transforms raw data obtained from camera sensors into an image that satisfies the requirements of a specific application or use case. An ISP typically has many tuning parameters due to the complexity of the image transformation. Until now, these are generally tuned by human experts manually, and this work takes a great deal of time. This paper proposes an application-level automatic ISP parameter tuning system. In particular, this paper focuses on a rear view monitoring (RVM) camera that is mounted on the rear side of the vehicle to prevent backovers in advanced driving assistance systems (ADAS). The proposed system consists of four steps. The first step is the input image generation, which captures a virtual scene including the test site and vehicle body whose three-dimensional (3D) models are created according to the test requirements and vehicle design. The second step is ISP processing, which transforms the input image into an ISP output image (RVM image) according to the ISP specification in the RVM system. The third step is to evaluate the RVM image's fitness using evaluation criteria (EC) functions. Finally, ISP parameters are tuned by the grid-to-random search method. In the experiment, the proposed system is evaluated by using the 3D modeling data of six different test vehicle types. Experimental results show that the proposed system can effectively obtain the usable ISP parameters' values that satisfy all RVM requirements for a given situation, regardless of test vehicle type, within 2~3 hours.

**INDEX TERMS** Automatic parameter tuning, grid-to-random search, image signal processor (ISP), rear view monitoring camera.

## I. INTRODUCTION

An image signal processor (ISP) is a dedicated processor that transforms raw data obtained from camera sensors into an image that satisfies the requirements of a specific application or use case. An ISP performs a role that reduces the workload of the central processing unit (CPU) by being in charge of pre-processing or post-processing of the image. Therefore, it is an indispensable part of the real-time embedded implementation of image-related products. An ISP has many tuning

parameters, and it is a very critical and difficult problem to set these parameters to appropriate values. ISP parameter tuning can be divided into three levels depending on its purpose: Image quality-level, computer vision algorithm-level, and application-level.

Image quality-level tuning is to find the optimal values of ISP parameters that generate an image suitable for the human visual system on a device that captures or displays an image such as a webcam, a mobile phone camera, and so on. This includes color demosaicking, denoising, white balance, color space conversion, tone mapping, and color enhancement [1]. At this time, general image quality is a research field that

The associate editor coordinating the review of this manuscript and approving it for publication was Senthil Kumar<sup>1</sup>.

has been studied for a long time and is evaluated by a metric often used for image quality assessment such as mean square error (MSE), signal-to-noise ratio (SNR), structural similarity index measure (SSIM) [2], visual SNR [3], subjective quality factor (SQF) [4], and so on [5]. Image quality-level tuning is currently the most common ISP parameter tuning.

Computer vision algorithm-level tuning is to find the optimal values of ISP parameters that maximize the performance of the computer vision algorithms such as object detection and image segmentation. How this controls image transformation is similar to that of image quality-level tuning. However, the difference is that the evaluation criterion is not visibility but the performance of the computer vision algorithm. For example, an ISP parameter tuning specialized for pedestrian detection algorithms can be applied for edge enhancement and contrast enhancement steps to maximize detection accuracy.

Finally, application-level tuning is to find the optimal values of the ISP parameters that generate an image that satisfies specific application requirements. For example, let's consider a camera/video image system (C/VIS) for heavy vehicles, which is a system that replaces side mirrors with cameras to minimize blind spots around the vehicle and provide an additional view that is difficult for the driver to acquire directly. C/VIS has an essential requirement that the size, position, and speed of objects captured by the camera remain the same as the mirror [6], [7]. However, there is no direct way to set the ISP parameters to transform the image to satisfy this requirement in the image quality-level and computer vision algorithm-level tuning. Therefore, it needs a way to use application-level requirements directly as evaluation criteria. Application-level ISP parameter tuning includes new components for image transformation, such as geometry transformation and image warping, and handles new ISP parameters such as field of view (FOV), zoom, scale, and shift. Moreover, it uses a new metric specialized to the application requirements as an evaluation measure for optimizing ISP parameters.

Typically, an ISP consists of several blocks of transformation and filtering to improve and modify the output image, and each block includes many ISP parameters. ISP parameter tuning is usually based on a manual tuning method in which a human expert adjusts the parameters repeatedly through trial and error until the fitness of the output image is satisfied. This manual tuning is a very cumbersome and time-consuming method. Recently, to overcome this problem, research on automating ISP parameter tuning is gradually increasing, and there is a research case [8] in which automatic tuning outperforms manual tuning.

Previous works on automatic ISP parameter tuning are at the early stages, and the number is relatively small. At the image quality-level tuning, previous works have proposed a method of automating ISP parameter tuning only for some basic processes such as denoising, demosaicking, and sharpening [3], [9], [10]. Nishimura *et al.* [9] proposed an automated ISP parameter tuning method for image quality.

The covered ISP consists of the four processing blocks, including noise reduction, demosaic, and sharpening, and ISP parameters consist of kernel size and coefficients used in each block. The optimal values of the ISP parameters are obtained by using Mean Absolute Difference and SSIM between the output image and the reference image as metrics. Portelli and Pallez [10] proposed an automatic ISP parameter tuning method for image enhancement. The covered ISP consists of noise reduction and sharpening, and ISP parameters consist of coefficients used in single filters. The optimal values of the ISP parameters are obtained by using visual noise and visual acutance as image quality metrics. Hevia *et al.* [3] proposed an automatic ISP parameter tuning method for image quality. The covered ISP consists of noise reduction and sharpening, and ISP parameters consist of denoise scales, denoise edge softness, weight, and so on. The optimal values of the ISP parameters are obtained by using modulation transfer function, visual SNR, and SQF as image quality metrics.

At the computer vision algorithm-level tuning, previous works mainly focused on computer vision algorithms utilized in the automotive field [8], [11], [12]. Yahiaoui *et al.* [11] proposed an automatic ISP parameter tuning method for improving pedestrian detection performance. The covered ISP consists of sharpening and contrast enhancement, and the ISP parameters consist of Laplacian filter's coefficients and clip limits of histogram equalization. Pedestrian detection performance is evaluated by intersection over unit (IOU), and the optimal values of the ISP parameters are obtained by using true positive rate and false positive per frame as detection results. Mody *et al.* [12] proposed an automatic ISP parameter tuning method to generate a high-quality image utilized in automated driver assistance systems (ADAS). The covered ISP parameters consist of analog gain, noise filter, sharpness, defect correction, and contrast, and the optimal values of the ISP parameters are obtained by using color accuracy as a measure. Mosleh *et al.* [8] proposed an automatic ISP parameter tuning method to improve the performance of the 2D object detection algorithm. The covered ISP consists of typical ISP blocks, and ISP parameters consist of parameters of most ISP blocks such as white balance, demosaicking, denoising, sharpening, and tone mapping. The optimal values of the ISP parameters are obtained by using mean average precision (mAP) and mean average recall (mAR) as object detection results and panoptic quality as panoptic segmentation results.

To the best of our knowledge, there is no prior work for automatic ISP parameter tuning at the application level. This paper proposes an application-level automatic ISP parameter tuning system. In particular, we focus on a rear-view camera used in rear view monitor (RVM) system that is designed to prevent backovers in ADAS. An RVM system provides a rear blind spot image that drivers cannot obtain directly. RVM images should meet the requirements presented in federal motor vehicle safety standard (FMVSS) No. 111 [13]. FMVSS No. 111 is a standard guideline for rear

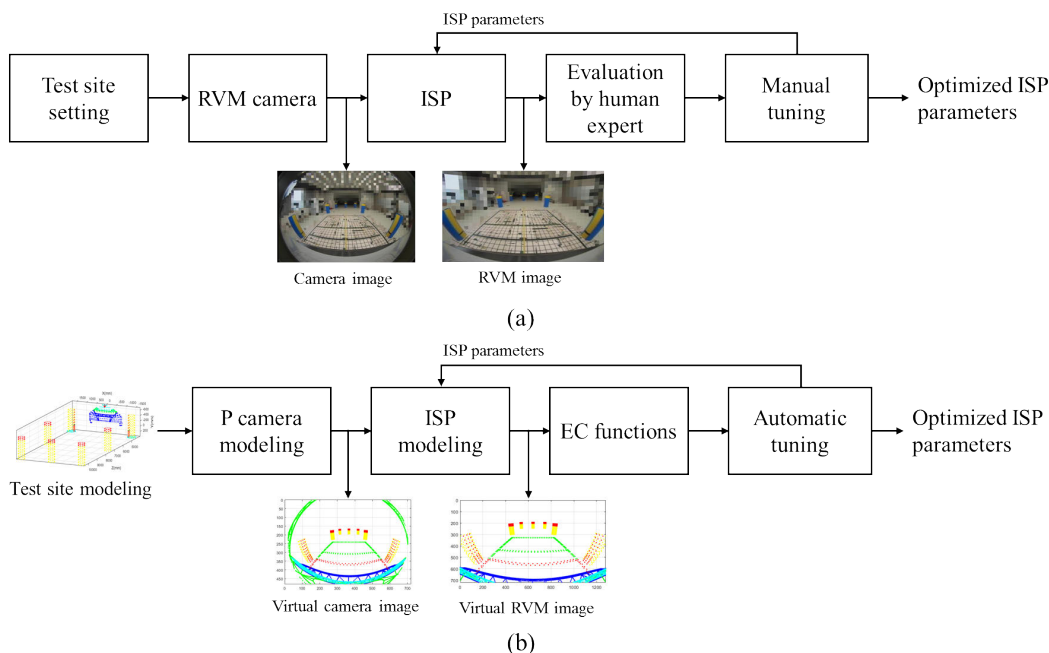


FIGURE 1. Overall process of RVM camera ISP parameter tuning: (a) manual tuning, (b) proposed automatic tuning.

visibility proposed by the National Highway Traffic Safety Administration (NHTSA).

In the case of manual tuning, it absolutely needs to set up a test site in advance, consisting of a test vehicle with a rear-view camera, 7 test objects, a fixed trajectory guideline, and so on. Furthermore, a human expert should iteratively perform the ISP parameter adjustment until the usable value is obtained while checking whether the output image satisfies the RVM application requirements. During the iterative task, the human expert should measure the length or area of the test object captured in the image by a pixel to determine the fitness of each output image while adjusting the values of ten or more ISP parameters related to lens distortion correction and image warping. In addition, if the test vehicle type, camera specification, or camera mounting location changes, the entire ISP tuning process must be repeated in the same manner for the new situation. Thus, manual tuning is a very cumbersome task that requires considerable effort and time. To alleviate the complexity of manual tuning, this paper proposes a system that automatically and efficiently tunes the ISP parameters regardless of vehicle types and camera specifications by simulating the test site and modeling the physical rear-view camera and the entire ISP processing. Fig. 1 shows a comparison of the typical manual tuning process and the proposed automatic tuning process.

The proposed system is composed of four steps. In the first step, the test site environment is modeled in 3D, and the input image is captured with a virtual camera. In the second step, the input image is transformed into an ISP output image (RVM image) specified by a set of ISP parameters. In the third step, the fitness of the RVM image is evaluated

by evaluation criteria (EC) functions that reflect the RVM application requirements. In the last step, the usable ISP parameters are obtained by the grid-to-random search-based parameter optimization method.

In the experiment, the proposed system is evaluated using 3D modeling data of 6 different vehicle types. Experimental results show that the proposed automatic tuning system can effectively obtain the ISP parameter values that meet all RVM application requirements for a given situation, regardless of vehicle type, within 2~3 hours. The proposed system is designed to enable tuning regardless of vehicle type and camera specifications and includes several useful functions required in actual tuning situations, such as checking intermediate results, saving intermediate results, and stopping tuning in the middle.

## II. APPLICATION REQUIREMENTS OF REAR VIEW MONITORING CAMERA

### A. CONFIGURATION OF THE TEST SITE

Configuration of the test site presented in FMVSS No.111 is as shown in Fig. 2. Seven cylindrical test objects are located at the positions behind the vehicle named A through G. The test objects have different markings according to their positions as shown in Fig. 3. The test objects at positions A to E are marked with a horizontal stripe of 150mm width in the top of the cylinder, as shown in Fig. 3(a).

The test objects at positions F and G are marked with a vertical stripe of 150mm width from the top to bottom of the cylinder, as shown in Fig. 3(c). In addition to the requirements of FMVSS No. 111, a fixed trajectory

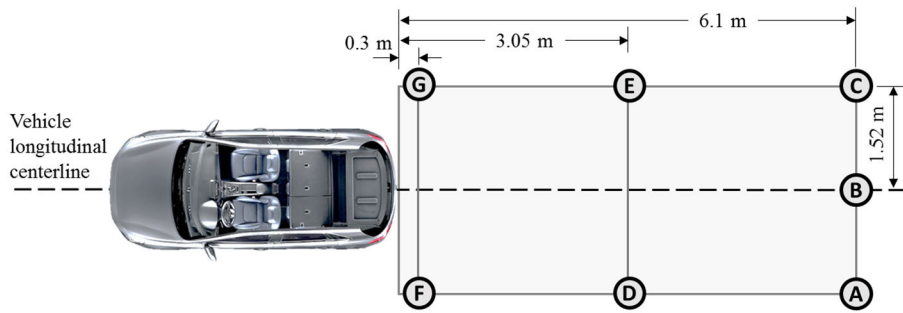


FIGURE 2. Arrangement of the test vehicle and test objects at the test site presented in FMVSS No. 111.

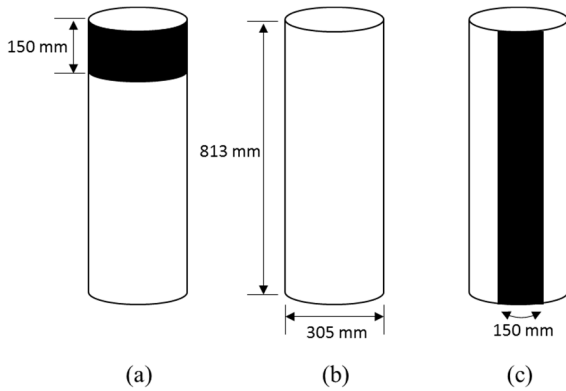


FIGURE 3. The dimensions and markings of test objects: (a) horizontal stripe marking, (b) test object dimension, (c) vertical strip marking.

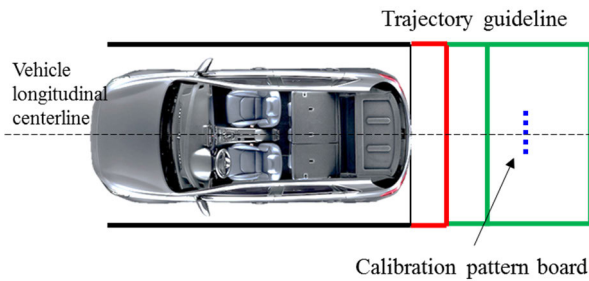


FIGURE 4. Arrangement of a fixed trajectory guideline and a calibration pattern board at the test site according to the customer's requirements.

guideline and a calibration pattern board are installed at the test site according to the customer's requirements, as shown in Fig. 4.

**B. APPLICATION REQUIREMENT DETAILS**

RVM application requirements consist of FMVSS No. 111 [14] and additional customer's requirements. Table 1 explains the details for two types of requirements.

**III. RVM IMAGE ACQUISITION**

In manual tuning, the RVM image acquisition process consists of test site setting, RVM camera, and ISP. In order to implement this process identically, the proposed automatic

TABLE 1. RVM application requirements.

Requirements in FMVSS No. 111	
Field of view	<ul style="list-style-type: none"> <li>- RVM image should display a minimum of a 150-mm wide portion along the circumference of each test object located at positions F and G. (The entire vertical stripe need not be visible.)</li> <li>- RVM image should display the full width and height of each test object located at positions A through E.</li> <li>- Reverse guideline overlays in the monitor must not cover any of the required portions of the test objects.</li> </ul>
Image size	<ul style="list-style-type: none"> <li>- All three test objects located at positions A, B, and C should average not less than 5 minutes of arc.</li> <li>- Each individual test object (A, B, and C) should not be less than 3 minutes of arc.</li> </ul>
Customer's requirements	
Vehicle body	<ul style="list-style-type: none"> <li>- RVM image should display the portion of a test vehicle bumper less than 10% of the entire image.</li> <li>- The vehicle body, such as trunk or garnish, should not appear at the top of the RVM image.</li> </ul>
Fixed trajectory guideline	<ul style="list-style-type: none"> <li>- A fixed trajectory guideline should be located at the center of the RVM image.</li> </ul>
Calibration pattern board	<ul style="list-style-type: none"> <li>- The ratio of the vertical length to the horizontal length of the pattern board should be as close as 1 as possible in the RVM image.</li> </ul>
Image size	<ul style="list-style-type: none"> <li>- The image size requirements of FMVSS No. 111 are interpreted as follows: The ratio (‰) of the horizontal stripe of the test object located at position B should be close to the defined threshold.</li> </ul>

tuning system is designed with the following three corresponding steps: 3D modeling for the test site, RVM camera modeling, and ISP modeling. Fig. 5 shows the corresponding

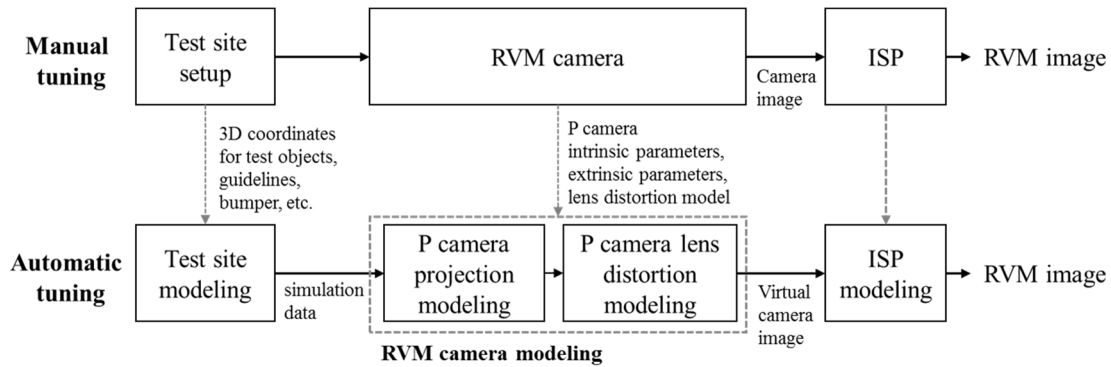


**FIGURE 5.** Diagram of the corresponding relationship between manual tuning and the proposed automatic tuning for the RVM image acquisition process.

relationship between manual tuning and the proposed automatic tuning as a diagram.

### A. TEST SITE MODELING

The test site is modeled based on the coordinate system where X-axis is the driver’s seat direction, the Y-axis is the ground direction, and the Z-axis is the vehicle’s backward direction. 3D model data for vehicle bodies (bumper, garnish, and trunk), a rear-view camera, cylindrical test objects, a fixed trajectory guideline, and a calibration pattern board are identically created as an actual test site by a simulation tool, as shown in Fig. 6. The simulated data are composed of 3D coordinate points that make up the mesh. These are created before tuning according to the vehicle type and camera specifications.

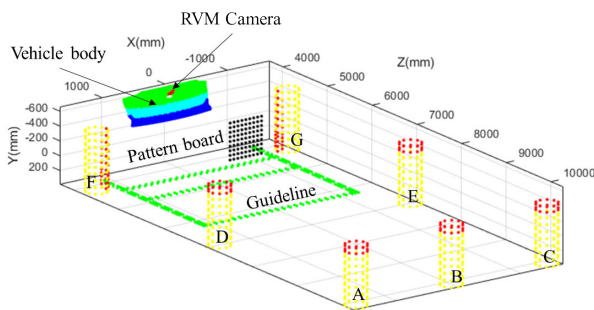


**FIGURE 6.** Test site modeling.

### B. RVM CAMERA MODELING

For automatic tuning, it needs to model a virtual camera (referred to as P camera in this paper) that replaces a rear-view camera. The P camera model is created using the intrinsic and extrinsic parameters of an actual rear-view camera. The RVM system generally uses a fisheye-lens camera. So, P camera’s lens distortion is modeled using the most commonly used equidistance projection model [15], [16].

Firstly, it performs to project a 3D data for the test site to P camera using the perspective projection model. If  $\mathbf{P}$  is a projection matrix that transforms a point  $(X, Y, Z)$  on the

world coordinate system to a point  $(x, y)$  on the image plane, the projection formula is as follows:

$$\begin{bmatrix} x \\ y \\ 1 \end{bmatrix} = \mathbf{P} \begin{bmatrix} X \\ Y \\ Z \\ 1 \end{bmatrix} \quad (1)$$

$[x \ y \ 1]^T$  is a vector representing a point on the homogeneous image coordinate system, and  $[X \ Y \ Z \ 1]^T$  is a vector representing a point on a homogeneous world coordinate system. The projection matrix  $\mathbf{P}$  is decomposed as follows:

$$\mathbf{P} = \mathbf{K} [\mathbf{R}|\mathbf{t}] = \begin{bmatrix} f_x & 0 & c_x \\ 0 & f_y & c_y \\ 0 & 0 & 0 \end{bmatrix} \begin{bmatrix} r_{11} & r_{12} & r_{13} & t_x \\ r_{21} & r_{22} & r_{23} & t_y \\ r_{31} & r_{32} & r_{33} & t_z \end{bmatrix} \quad (2)$$

$\mathbf{K}$  is an intrinsic parameter matrix of the camera and the rigid transformation  $[\mathbf{R}|\mathbf{t}]$  is an extrinsic parameter matrix of the camera.

To reflect a fisheye lens distortion on the P camera model, the equidistance projection model is applied for a point on the image plane obtained by a perspective projection model. The equidistance projection model is calculated as follows:

$$r_d = f\theta \quad (3)$$

$r_d$  is a distance from a principal point to a point on an image plane,  $\theta$  is an incidence angle of light from the object based on the optical axis, and  $f$  is a focal length. The equidistance projection result can be obtained from the perspective projection result as follows:

The first is to calculate the incidence angle of light from the coordinates of the perspective projected image points using the relationship between the two models. The second is to calculate the distance  $r_d$  between the image point and the principal point by substituting the incidence angle  $\theta$  and the given focal length into equation (3). If the  $x$  and  $y$  coordinates of the fisheye projection image are calculated from  $r_d$ , a final fisheye projection image can be generated. Fig. 7 shows the actual image taken from a rear-view camera and the virtual image acquired from the P camera.

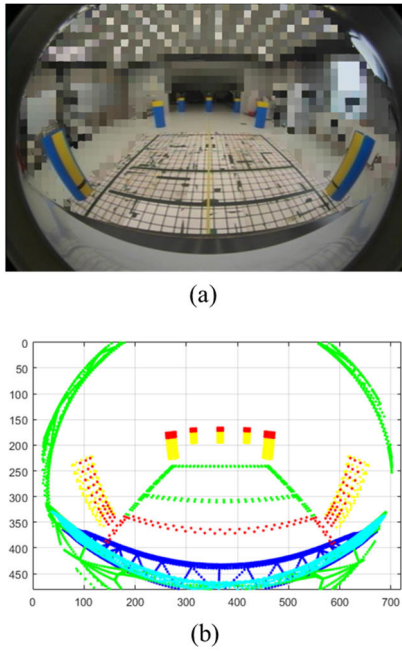


FIGURE 7. Comparison between an actual camera image and a virtual camera image: (a) actual fisheye lens camera image, (b) P camera image.

IV. ISP MODELING

To model ISP functions, this paper assumed the following two camera models: A camera (meaning an actual camera) model and V camera (meaning a virtual camera) model. That is, it was assumed that the input image was acquired with the A camera, and the resulting image was taken with the V camera to generate an output image, as shown in Fig. 8. In other words, the ISP undertakes a conversion from A camera to V camera, which is composed of fisheye lens distortion correction and virtual pan-tilt-zoom (PTZ). Since the P camera substitutes for a role of the actual fisheye lens camera, the P camera output image (i.e., ISP input image) contains fisheye lens distortion. The lens distortion correction facilitates subsequent geometric transformation by eliminating this distortion. Fig. 9 shows the fisheye lens distortion correction process except for virtual PTZ. Here, it should be noted that the lens distortion correction in our ISP model is not aimed at generating a perfect pinhole camera image as is generally done in the field of computer vision. It may be physically impossible to transform a rear-view camera image with an ultra-wide view into a perfect pinhole camera image. Since the fisheye lens distortion correction here aims to improve the driver’s situational understanding by displaying the output image on a monitor with a limited size, it is not

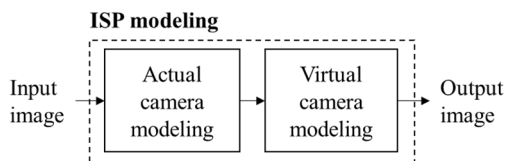


FIGURE 8. ISP modeling.

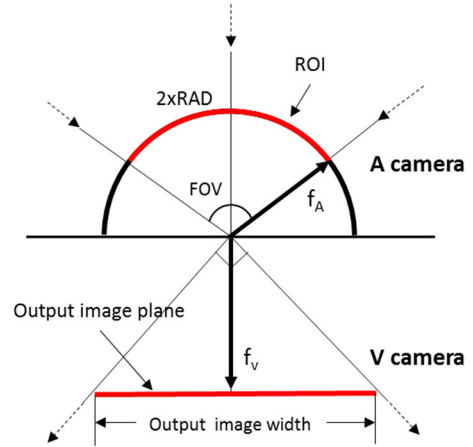


FIGURE 9. Fisheye lens distortion correction in the ISP model.

TABLE 2. ISP parameters for the RVM camera.

Parameter	Default value	Range	Unit
FOV	180	-	Degrees
RAD	640	-	
H shift ( $x_{is}$ )	0	-	
V shift ( $y_{is}$ )	0	-	
H Pan ( $\theta_{cv}$ )	0	[0...180]	Degrees
V Pan ( $\phi_{cv}$ )	0	[-180...180]	Degrees
Zoom ( $r_{cv}$ )	1	[0.01...10]	
Tilt ( $\alpha_{sz}$ )	0	[-180...180]	Degrees
Advanced H shift ( $x_{os}$ )	0	[-1...1]	
Advanced V shift ( $y_{os}$ )	0	[-1...1]	
Advanced H scale ( $s_{os}$ )	1	[0.5...2]	
Advanced V scale ( $s_{ov}$ )	1	[0.5...2]	
Theta ( $\theta_{st}$ )	0	[0...180]	Degrees
Phi ( $\phi_{st}$ )	0	[-180...180]	Degrees

important whether it is a perfect pinhole camera image, but whether it meets the RVM application requirements. Virtual PTZ simulates that a real PTZ camera captures scenes in different directions and different magnifications according to pan, tilt, and zoom. In general, the virtual PTZ receives a high-resolution wide-angle image and outputs the part corresponding to the parameter of the PTZ camera. In this paper, the pan, tilt, zoom, pose (theta, phi), and image offset of the virtual image plane are considered as shown in Fig. 10. Fig. 10 shows the virtual PTZ with the fisheye lens distortion effect removed, and Table 2 summarizes ISP parameters for the fisheye lens distortion correction and virtual PTZ.

Table 3 shows the effect of each ISP parameter on the image transformation operating inside the ISP. In the A camera lens view column of Table 3, the area in the input

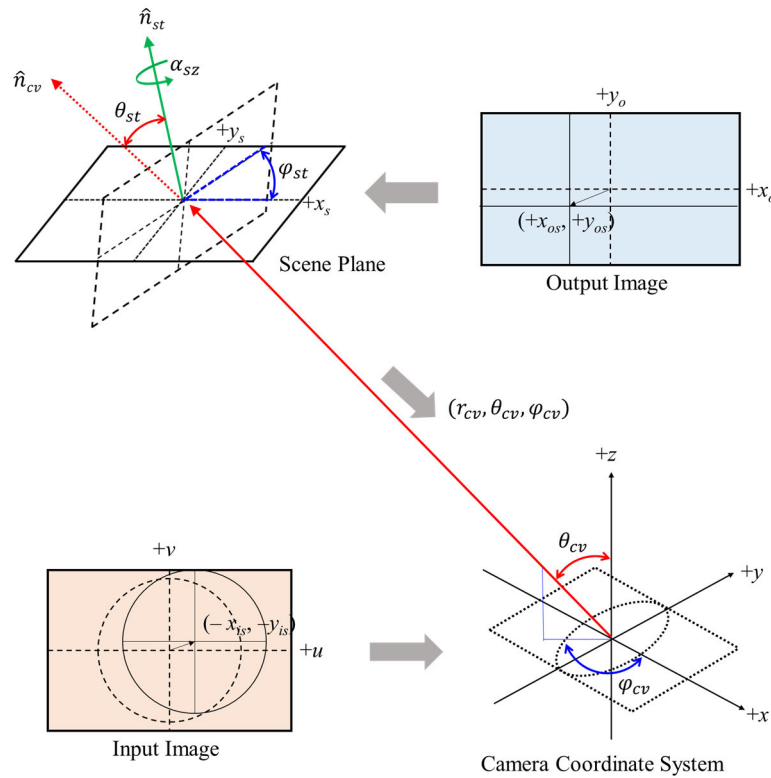


FIGURE 10. Virtual PTZ in the ISP model.

image corresponding to the output image (RVM image) is represented by a green line. The FOV and RAD determine the size of the ROI, which is the area (enclosed by green line) to be used as the output image. V shift and H shift moves the position of the ROI vertically and horizontally. Zoom functions to enlarge or reduce the image. Advanced H shift, V shift, H scale, and V scale function to finely adjust the shape and position of the ROI. The remaining H pan, V pan, and Tilt determine the orientation direction of the virtual PTZ camera, and Advanced theta and phi determine the pose of the image plane. In this paper, according to the customer’s requirements, 5 ISP parameters (H pan, V pan, Tilt, Theta, and Phi) related to angle are fixed to zero and only the remaining 9 parameters are dealt with.

**V. EVALUATION CRITERIA FUNCTION**

Evaluation criteria (EC) functions are defined as a measure to quantitatively evaluate how well a specific ISP parameter satisfies the RVM application requirements. The EC functions consist of EC functions for FMVSS No.111 and EC functions for customer’s requirements (regarding vehicle body, a fixed trajectory guideline, and a pattern board). Each EC function is defined so that the corresponding requirements are reflected, and results of EC functions will be summarized into one number, i.e., final score (called an EC score). The details of the EC functions are as follows.

EC function 1 is a function that evaluates the requirements of FMVSS No.111 and consists of four sub-EC functions

related to FOV and image size. The contents of the four sub-EC functions are as follows (Fig. 11):

- 1-1) Check whether the lower 150 mm × 150 mm area of the vertical stripe marked on the test objects located at the positions F and G (the rectangular area connected to the corners ③ to ⑥ in Fig. 11) is visible in the RVM image. Outputs 1 if it is visible, and 0 otherwise.
- 1-2) Calculate the area of the vertical stripe of the test objects located at the positions F and G in the RVM image (the rectangular area connected to ① - ② - ③ - ④ - ⑤ - ⑥ - ① in Fig. 11). The larger the ratio (%) of the calculated area to the entire area of the RVM image, the better.
- 1-3) Find the position of the top point among the test objects located at positions A, B, and C and calculate the vertical distance *d* from that point to the top of the image. Next, the ratio of *d* to the vertical length of the image must be 15% or more.
- 1-4) Calculate the area of the horizontal stripe of the test object located at the position B (*w* × *h*). The larger the ratio (%) of the calculated area to the entire area of the RVM image, the better.

EC function 2 is a function that evaluates the customer’s requirements and consists of four sub-EC functions related to vehicle body conditions. The contents of the four sub-EC functions are as follows (Fig. 12):

TABLE 3. Effect of ISP parameters on image transformation.

ISP parameter value	A camera lens view	Output image	ISP parameter value	A camera lens view	Output image
Default values			Default values		
FOV: 240°			RAD: 320 Tilt: 45°		
RAD: 320			FOV: 240° Advanced H shift: 0.5		
RAD: 320 V shift: 100			FOV: 240° Advanced V shift: 0.5		
RAD: 320 H shift: 100			FOV: 240° Advanced H scale: 1.5		
RAD: 320 H Pan: 50°			FOV: 240° Advanced V scale: 1.5		
RAD: 320 H Pan: 50° V Pan: 90°			FOV: 240° Advanced Theta: 30°		
Zoom: 2			FOV: 240° Advanced Theta: 30° Advanced Phi: 90°		

- 2-1) Measure the vertical length ( $t_c$ ) of the bumper at the center of the horizontal axis of the RVM image. It is preferred that the ratio (%) of  $t_c$  to the vertical length of the RVM image is between 4 and 8 %.
- 2-2) Calculate the average of the vertical lengths  $t_l$  and  $t_r$  of the bumper at the left and right ends of the RVM image. It is preferred that the ratio (%) of the average value to the vertical length of the RVM image is between 8 and 16%.

- 2-3) The smaller the difference between the vertical lengths  $t_l$  and  $t_r$ , the better.
- 2-4) Checks whether a vehicle body such as a garnish or trunk is visible on the upper part of the RVM image. Outputs 0 if visible, and 1 otherwise.

EC function 3 is a function that evaluates the customer's requirements and consists of two sub-EC functions related to the fixed trajectory guideline. The contents of the two sub-EC functions are as follows (Fig. 12):



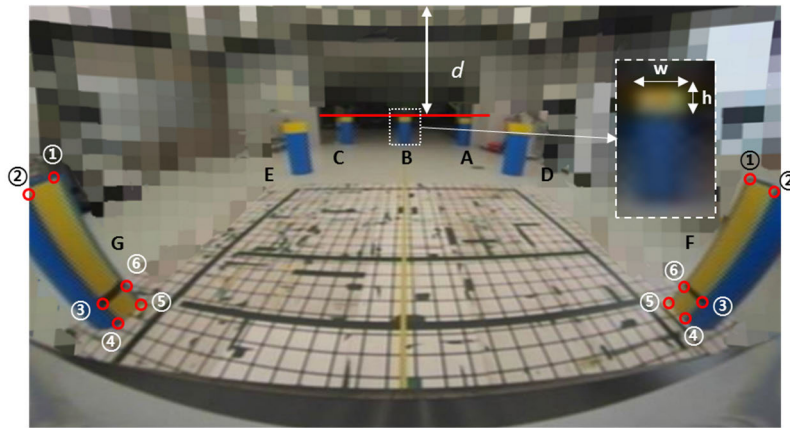


FIGURE 11. Description of EC function 1 related to the requirements of FMVSS No.111.

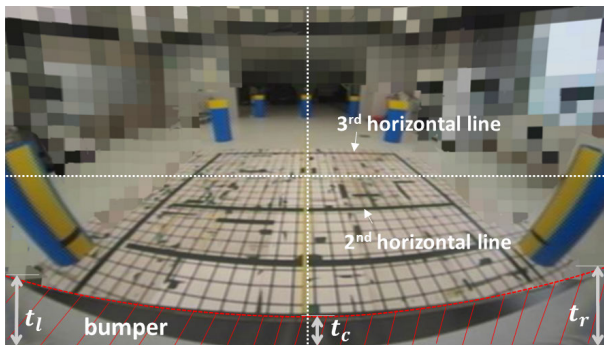


FIGURE 12. Description of EC function 2 and 3 related to customer's requirements.

- 3-1) Calculate the distance between the  $X$  coordinate of the center point of the second horizontal guideline from the rear of the vehicle and the  $X$ -axis center coordinate of the RVM image. The smaller the calculated distance, the better.
- 3-2) Calculate the  $Y$  coordinate of the center point of the third horizontal guideline from the rear of the vehicle. It is preferred that the ratio (%) of the calculated  $Y$  coordinate to the vertical length of the RVM image is between 45 and 55%.

EC function 4 is a function that evaluates the customer's requirements and consists of one sub-EC functions related to the calibration pattern board. The content of the sub-EC function is as follows:

- 4-1) It is preferred that the ratio of the width to the height of the calibration pattern board is between 0.9 and 1.1.

The outputs of the EC functions are set to convert the values measured in the function into a score of 0 or 1 based on the threshold value determined by a human expert. However, if using the EC functions outputting a binary score, it is impossible to search usable (even not perfect) ISP parameters when there is no perfect ISP parameter values. Frequently,

what the operator really wants to do is to find the best ISP parameter values under a given conditions. In order to solve this problem, we propose a method to apply a sigmoid function to the output stage of each EC function so that all EC functions output real numbers between 0 and 1. However, since most of the EC functions defined in this paper have two thresholds (maximum and minimum values), it is difficult to use the sigmoid function having a single threshold as it is. Therefore, a bidirectional sigmoid function with two thresholds was proposed by combining two basic sigmoid functions as shown in (4).

$$f(x) = \frac{1}{1 + e^{-c_1 \times (x - c_2)}} \times \frac{1}{1 + e^{c_3 \times (x - c_4)}} \quad (4)$$

$c_1$  and  $c_3$  represent the slope of each sigmoid function,  $c_2$  and  $c_4$  represent the minimum and maximum thresholds, respectively, and the graph of the bidirectional sigmoid function is shown in Fig. 13. In the case of an EC function with one threshold,  $c_2$  or  $c_4$  is set to infinity. In this paper, the proposed bidirectional sigmoid function is placed at the output stage of eleven EC functions, and all functions are set to output real numbers between 0 and 1. The coefficients of the bidirectional sigmoid function are set differently for each

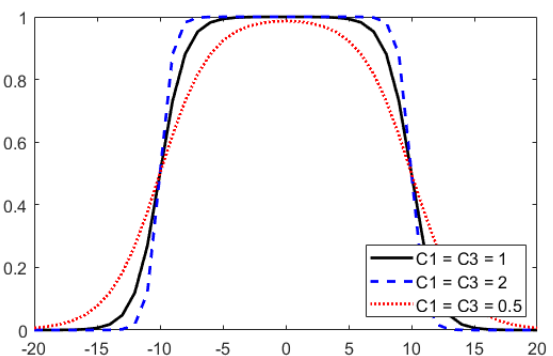
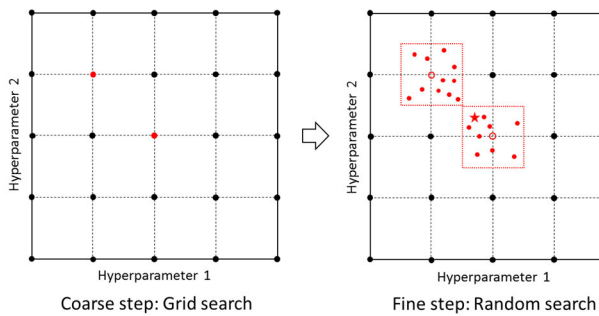


FIGURE 13. Graphs of bidirectional sigmoid functions with different slopes when  $c_2$  is -10 (minimum value) and  $c_4$  is 10 (maximum value).

EC function according to the customer’s decision. The EC score is calculated as the product of all EC function outputs.

**VI. ISP PARAMETER OPTIMIZATION**

This paper proposes a grid-to-random search method to optimize the ISP parameters. This method consists of two steps, coarse search and fine search, as shown in Fig. 14. In the coarse search step, grid search is performed sparsely by assigning relatively large values to the search range and step size. First, the parameter space is divided into a grid using the ISP parameter initial value, search range, and step size, and then ISP parameter candidate sets are generated. Next, the EC function results for the parameter candidate sets are sequentially calculated. To this end, according to each candidate parameter set, an RVM image is generated and an EC score is calculated by applying all EC functions to the image. EC scores for all candidate sets are sorted in descending order, and the top *N* parameter sets are output as the result of the coarse search step. Here, *N* is the number of parameter sets that are obtained in the coarse search step. The *N* ISP parameter sets obtained in the coarse search step become the initial values of the ISP parameters in the fine search step.



**FIGURE 14. Proposed ISP parameter optimization method.**

In the fine search step, random search is performed densely by assigning relatively small values to the search range and step size. It is well known that random search is advantageous in optimizing high-dimensional parameters because it has more search times than grid search in the important parameter axis when using the same amount of computation [17]. Furthermore, random search has the advantage that it is possible to check the intermediate result during the search process and stop the search at any time. For this reason, the random search was applied in the fine search step. In the fine search step, the ISP parameter candidate sets are generated randomly as much as the specified number of searches (*T*) within the fixed search range. According to each candidate parameter set, an RVM image is generated and an EC score is calculated by applying all EC functions to the image. EC scores for all candidate sets are sorted in descending order, and the top *M* parameter sets are output as the result of the fine search step. Finally, one final parameter set among the *M* candidates is determined by human expert.

**VII. EXPERIMENTS**

The proposed system was evaluated with 3D simulation data of six vehicle types. These data consist of rear-view camera (P camera) parameters and 3D coordinates for vehicle bodies, cylindrical test objects, a fixed trajectory guideline, and a calibration pattern board. Test vehicles are composed of six different types, and body shape and the mounting position of the rear-view camera are different according to the type of vehicle. Vehicles A, B, C, and F are sedans, and vehicles C and E are sport utility vehicles (SUVs). Fig. 15 shows 3D simulation data for four test vehicles from A to D. Test vehicles E and F, which are unreleased models, are not included in this figure due to security concerns.

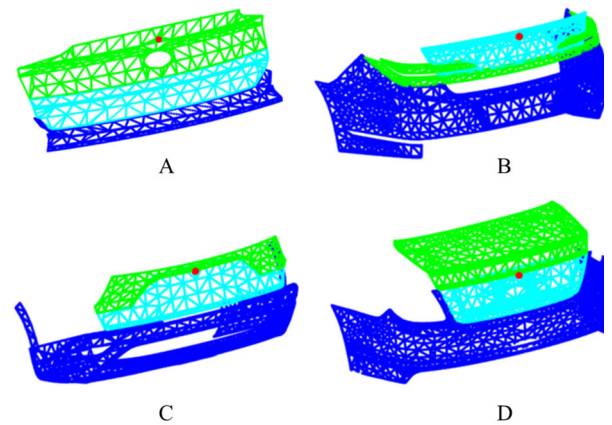


**FIGURE 15. 3D simulation data for four test vehicles (red point: rear-view camera, blue: bumper, green: garnish, light blue: trunk).**

**A. OPTIMIZATION PARAMETER SETTING**

The proposed ISP parameter optimization method needs to set up optimization parameters that consist of the number of outputs (*N*) of the coarse search step and the number of searches (*T*) of the fine search step. These two parameters determine how many initial positions are to be searched for in the fine step and how many are needed to search around the initial positions, and as a result, they can influence the search time and the fitness of the RVM image. In the actual situation, a human expert will set the optimization parameters according to the given situation, but in this paper, the parameters are set empirically to derive the experimental results within the allowable range of processing time and performance. In order to set the optimization parameters, we performed an experiment to measure the EC score and processing time by changing the number of coarse steps results (*N*) and the number of fine steps searches (*T*) for one vehicle type (test vehicle A). Fig. 16(a) shows EC scores according to *N*, and also EC scores when the *T* (legend number) is different. In this paper, the threshold (=0.002) set within the acceptable range determined by the customer’s expert is indicated by a solid horizontal line. As shown in Fig. 16(a), it can be seen that the tendency of increasing or decreasing EC scores according to

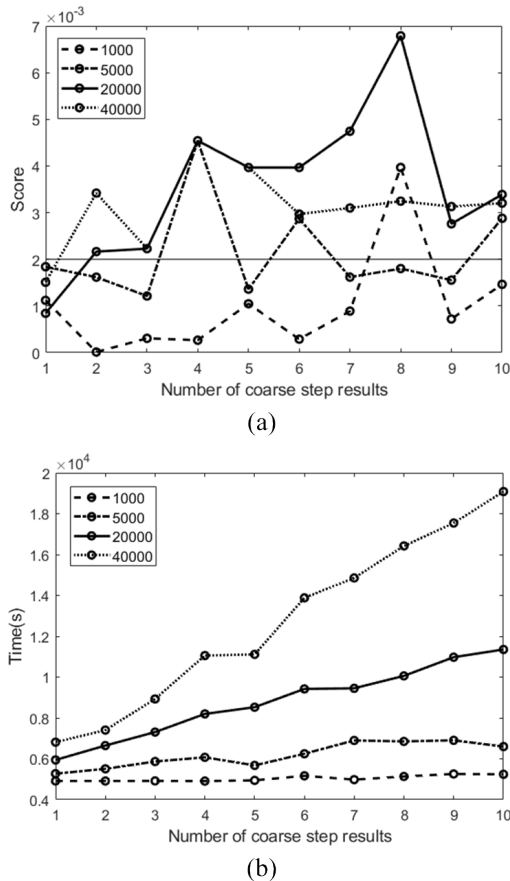


**FIGURE 16.** Graphs for EC score and processing time: (a) EC scores according to optimization parameters for test vehicle A, (b) processing time according to optimization parameters for test vehicle A.

optimization parameters  $N$  and  $T$  does not appear clearly due to the influence of random search performed in the fine step. However, when  $N$  and  $T$  is 1 and 1000 respectively, the EC scores are smaller than the threshold, and when  $T$  is more than 20000, the EC scores are greater than the threshold. On the other hand, in the case of the processing time, it can be seen that the processing time increases as  $T$  increases, as shown in Fig. 16(b). Based on these results, the optimization parameter was set so that the search time was minimized while the EC score is stably obtained more than the threshold, as shown in Fig. 16(a). In our experiments,  $N$  is set to 2, and  $T$  is set to 20000.

**B. ANALYSIS OF EC FUNCTION RESULTS FOR RVM IMAGE OF THE TEST VEHICLE A**

The result of each EC function for the RVM image obtained from the proposed ISP tuning system was analyzed. The four EC functions (EC 1-1, 1-2, 1-3, and 1-4) corresponding to the requirements of FMVSS No. 111 obtained high scores close to 1. Among the EC functions corresponding to the customer’s requirements, EC 2-3, 2-4, 3-1, and 4-1 obtained high scores close to 1, but EC 2-1, 2-2, and 3-2 obtained low scores less than 0.5. Checking the measured value of the EC function

that obtained a low score, the value is within the acceptable range offered by the customer’s experts. Nevertheless, the reason why the low score was obtained is analyzed by the influence of the coefficients of the bidirectional sigmoid function. In summary, all sub-EC functions of EC function 1 related to the essential requirements obtained high scores, and EC functions 2 to 4 related to customer’s requirements also obtained stable results within the range allowed by human experts.

**EC function 1: FMVSS No. 111 requirements**

- 1-1) Since the lower 150 mm  $\times$  150 mm portion of the vertical stripe of test objects located at positions F and G is visible in the RVM image, the score is 1 (Fig. 17(a)).
- 1-2) The area ratio of the vertical stripe of test objects located at positions F and G is 26.12%, and since this value is sufficiently large, the score is 1 (Fig. 17(b)).
- 1-3) The ratio of the length  $d$  is calculated as 25.70 %, and since this value is more than 15%, the score is 0.99 (Fig. 17(c)).
- 1-4) The area ratio of the horizontal stripe of test object located at position B is calculated as 0.2 %, and since this value is sufficiently large, the score is 0.91 (Fig. 17(d)).

**EC function 2: Customer’s requirements for vehicle body**

- 2-1) The ratio of the bumper’s vertical length at the center on the horizontal axis of the RVM image is calculated as 3.45 %, and since this value is less than 4%, the score is 0.16 (Fig. 18(a)).
- 2-2) The ratio of the average of the vertical lengths of the bumper at the left and right ends of the RVM image is calculated as 17.75%, and since this value exceeds 16%, the score is 0.009 (Fig. 18(a)).
- 2-3) The difference of the vertical lengths of the bumper at the left and right ends of the RVM image is measured as 1.08 pixel, and since this value is sufficiently small, the score is 0.99 (Fig. 18(a)).
- 2-4) Since the vehicle body such as a garnish or trunk is not included in the upper part of the area (area marked with red line in Fig. 18(b)) used as the RVM image, the score is 1.

**EC function 3: Customer’s requirements for a fixed trajectory guideline**

- 3-1) The distance between the  $X$  coordinate of the second horizontal guideline center point and the  $X$ -axis center coordinate of the image is measured as 0.09 pixels, and since this value is sufficiently small, the score is 0.99 (Fig. 19(a)).
- 3-2) The vertical length ratio of the  $Y$  coordinate of the third horizontal guideline is calculated as 55%, and since this value falls within the range of 45~55%, the score is 0.5 (Fig. 19(b)).

**EC function 4: Customer’s requirement for a calibration pattern board**

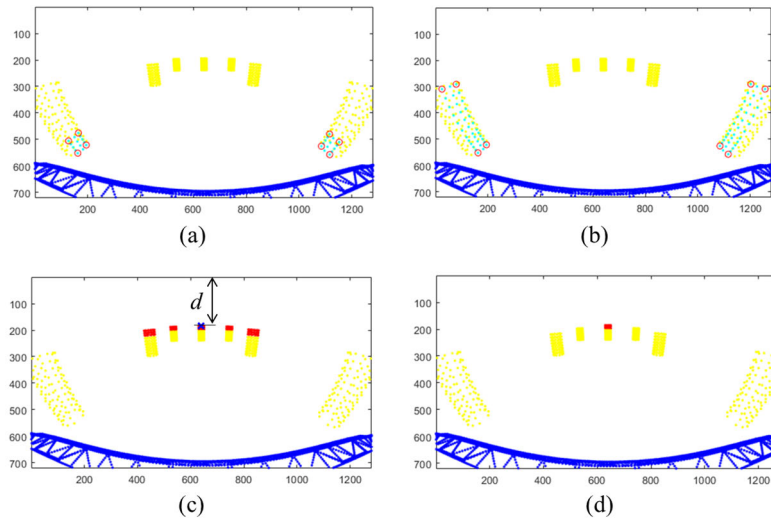


**FIGURE 17.** Results for EC function 1: (a) EC 1-1 result, (b) EC 1-2 result, (c) EC 1-3 result, (d) EC 1-4 result.

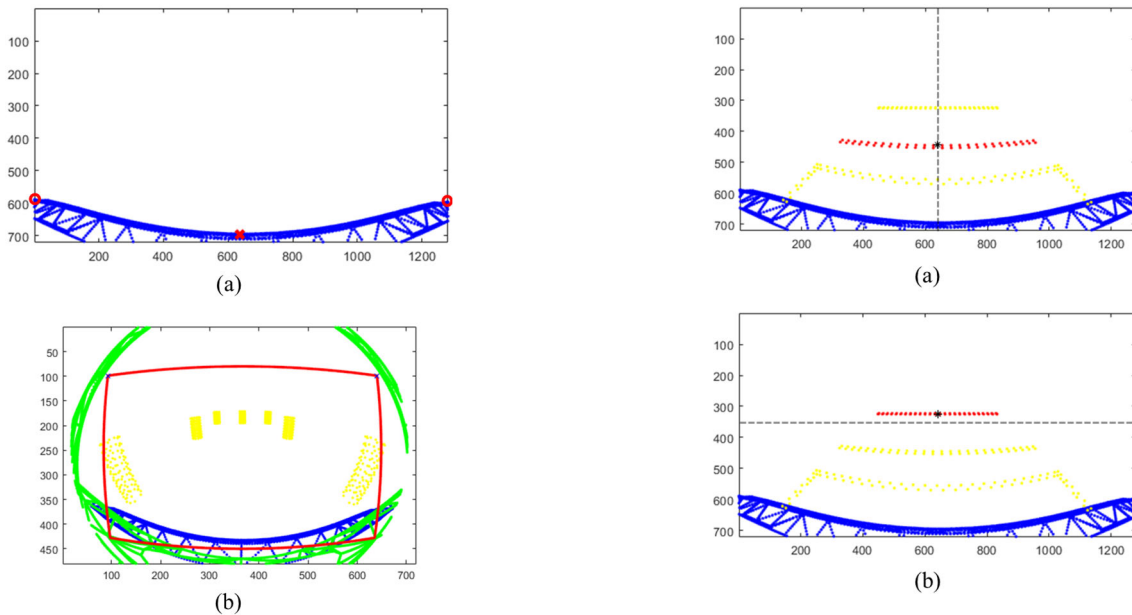
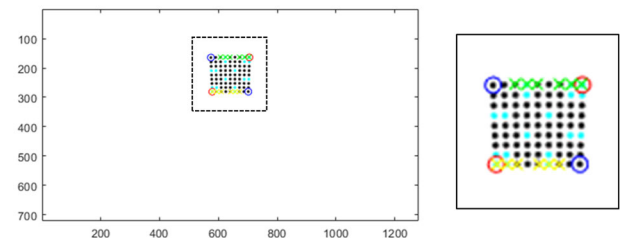


**FIGURE 18.** Results for EC function 2: (a) EC 2-1 result, (b) EC 2-2 result.

**FIGURE 19.** Results for EC function 3: (a) EC 3-1 result, (b) EC 3-2 result (dashed line: center line).

4-1) The ratio of the width and height of the calibration pattern board is calculated as 1.08, and since this value falls within the range of 0.9 to 1.1, the output value is 0.7 (Fig. 20).

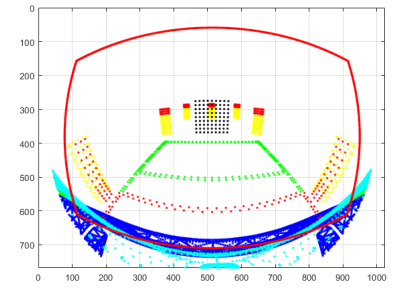
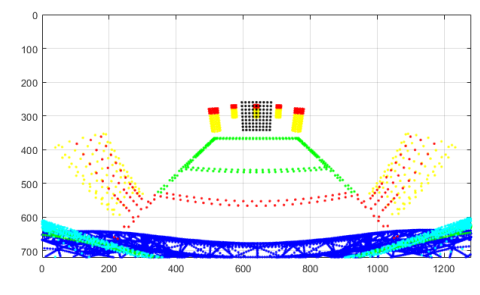
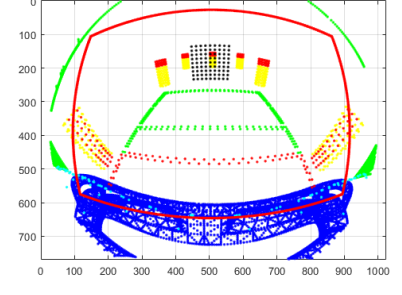
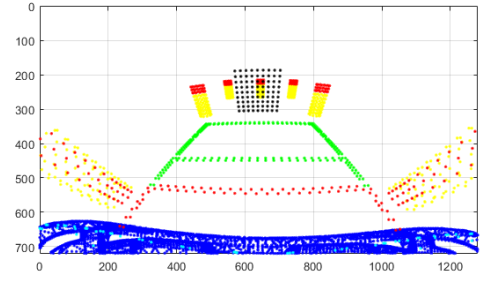
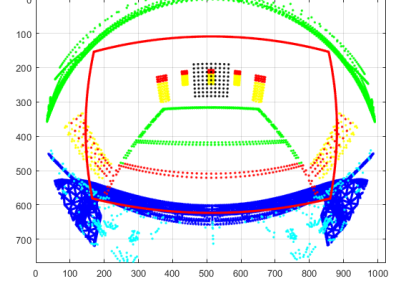
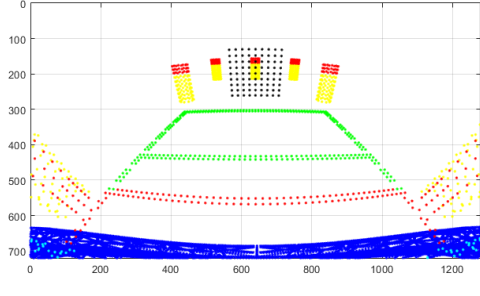
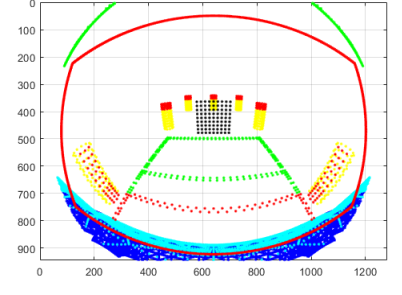
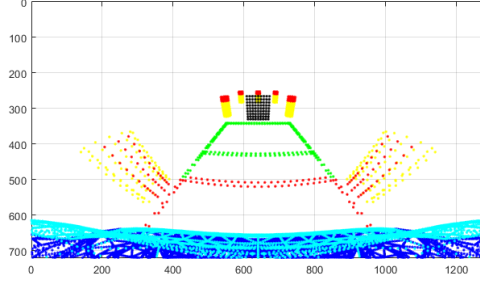
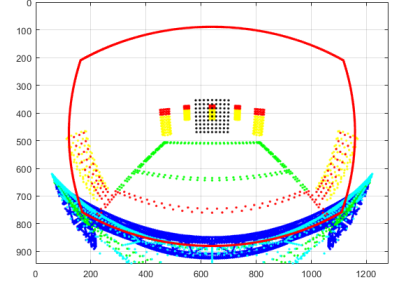
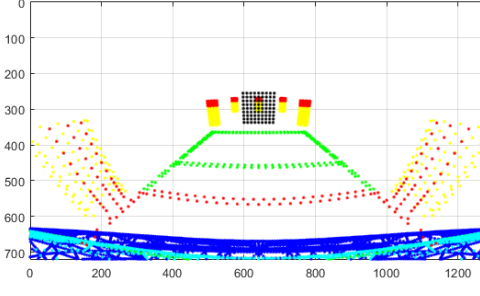
Finally, we compare actual images obtained by the actual camera and virtual images obtained from the proposed automatic ISP parameter tuning system. Fig. 21(a) and (b) show the input image captured in the actual test environment and the RVM image output through the ISP, respectively. Fig. 21(c) and (d) show the virtual image acquired by the P camera and the RVM image output by the ISP model, respectively. Comparing Fig. 21(a) and (c), it can be seen that



**FIGURE 20.** Results for EC function 4-1.

the virtual image is quite similar to the actual image. In the same manner, comparing Fig. 21(b) and (d), it can be seen that the RVM image obtained in the proposed system is also quite

**TABLE 4.** Input images and RVM images for five test vehicles.

Test vehicle	Input image and ROI	RVM image
B		
C		
D		
E		
F		

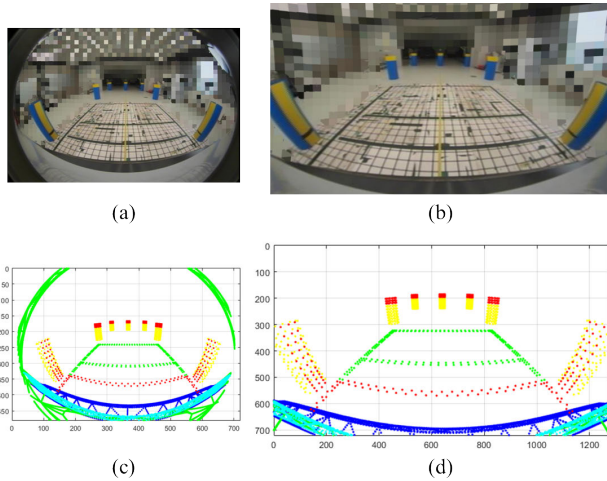


**FIGURE 21.** Input image and RVM image: (a) input image acquired by actual RVM camera mounted on real test vehicle, (b) RVM image obtained through ISP from an actual input image, (c) input image acquired by simulated P camera, (d) RVM image obtained through ISP model from a simulated input image.

similar to the actual RVM image. These results demonstrate that the proposed ISP parameter tuning system can provide usable ISP parameters that can be sufficiently applied in real vehicles.

### C. ISP PARAMETER OPTIMIZATION RESULTS FOR ANOTHER FIVE TEST VEHICLES

We performed ISP parameter optimization for another five vehicle types from B to F and obtained an RVM image for each vehicle type by using the resultant ISP parameters, as shown in Table 4. At first, the initial values of the ISP parameters and the optimization parameters are set the same as those of test vehicle A. Next, the ISP parameters for each test vehicle are automatically tuned by the proposed system. Finally, the RVM image is generated by using the resultant ISP parameters. Table 4 shows input images including a grid (red line) indicating an area used for the RVM image and resultant RVM images. As a result of the experiment, all five vehicle types satisfy all requirements of FMVSS No. 111. Also, customer's requirements are satisfied within the allowable range offered by human experts.

Since the six test vehicle types have different vehicle body shapes and different RVM camera mounting locations, the input images captured in different environments have different test object arrangements. Nevertheless, the proposed system can obtain the usable values of the ISP parameters suitable for each test vehicle in hours, regardless of vehicle types. These results demonstrate that the proposed system is quite efficient compared to manual tuning in terms of test site setting, repetitive labor given to human experts, and the working time. Finally, Table 5 shows the processing time for six vehicle types. The processing time was measured with an Intel Core i7-7700 CPU with 16.0GB RAM. Average tuning time of the six vehicle types is about 142 minutes. Considering that the human expert took 1~2 working days,

**TABLE 5.** Processing times for six test vehicles.

Vehicle type	Processing time (min)
A	110
B	161
C	127
D	134
E	188
F	130
average	142

it can be seen that the working time can be drastically reduced. As shown in Table 5, the reason why the processing time is different according to the vehicle type is that the number of points of the simulation data used is different. That is, as the number of data points increases, the processing time increases.

### VIII. CONCLUSION

This paper proposed an automatic system that searches the usable ISP parameter values for the rear-view camera to satisfy the requirements of the RVM application. For this, we developed an algorithm that automatically evaluates the fitness of the RVM image and searches usable values of the ISP parameters. Experimental results proved that the proposed system effectively reduces the effort and time required by improving the optimization performance of the ISP parameters and reducing the workload from 1~2 working days to several hours. In addition, the proposed system provides a method to check whether the camera specifications and locations can satisfy the requirements of the RVM application in the vehicle design stage before the actual vehicle is constructed. Future works include 1) automatic setting of parameters for bidirectional sigmoid functions, 2) normalization or automatic setting of EC function thresholds, and 3) dimension reduction of parameter space through analysis of dependency between ISP parameters.

### REFERENCES

- [1] Z. Liang, J. Cai, Z. Cao, and L. Zhang, "CameraNet: A two-stage framework for effective camera ISP learning," *IEEE Trans. Image Process.*, vol. 30, pp. 2248–2262, 2021.
- [2] Z. Wang, A. C. Bovik, H. R. Sheikh, and E. P. Simoncelli, "Image quality assessment: From error visibility to structural similarity," *IEEE Trans. Image Process.*, vol. 13, no. 4, pp. 600–612, Apr. 2004.
- [3] L. V. Hevia, M. A. Patricio, J. M. Molina, and A. Berlanga, "Optimization of the ISP parameters of a camera through differential evolution," *IEEE Access*, vol. 8, pp. 143479–143493, 2020.
- [4] *Acutance and SQF*. Accessed: Apr. 2021. [Online]. Available: <https://www.imatest.com/docs/sqf/>
- [5] *IEEE Standard for Camera Phone Image Quality*, Standard 1858-2016 (Incorporating IEEE Std 1858-2016/Cor), Jan. 2017, pp. 1–146.
- [6] W. W. Wierwille, W. A. Schaudt, J. M. Spaulding, S. K. Gupta, G. M. Fitch, D. M. Wiegand, and R. J. Hanowski, "Development of a performance specification for camera/video imaging systems on heavy vehicles," Final Rep. Specifications, Richmond, VA, USA, Tech. Rep. DOT HS 810, Jul. 2008, vol. 958.

- [7] A. Terzis, Ed., *Handbook of Camera Monitor Systems: The Automotive Mirror-Replacement Technology Based on ISO 16505*. Cham, Switzerland: Springer, 2016.
- [8] A. Mosleh, A. Sharma, E. Onzon, F. Mannan, N. Robidoux, and F. Heide, "Hardware-in-the-loop end-to-end optimization of camera image processing pipelines," in *Proc. IEEE/CVF Conf. Comput. Vis. Pattern Recognit. (CVPR)*, Jun. 2020, pp. 7529–7538.
- [9] J. Nishimura, T. Gerasimow, R. Sushma, A. Sutic, C.-T. Wu, and G. Michael, "Automatic ISP image quality tuning using nonlinear optimization," in *Proc. 25th IEEE Int. Conf. Image Process. (ICIP)*, Oct. 2018, pp. 2471–2475.
- [10] G. Portelli and D. Pallez, "Image signal processor parameter tuning with surrogate-assisted particle swarm optimization," in *Proc. Int. Conf. Artif. Evol.* in *Lecture Notes in Computer Science*, vol. 12052. Cham, Switzerland: Springer, 2019, pp. 28–41.
- [11] L. Yahiaoui, J. Horgan, B. Deegan, S. Yogamani, C. Hughes, and P. Denny, "Overview and empirical analysis of ISP parameter tuning for visual perception in autonomous driving," *J. Imag.*, vol. 5, no. 10, p. 78, Sep. 2019.
- [12] M. Mody, S. Dabral, M. Magla, H. Sanghvi, N. Nandan, K. Chitnis, B. Jadhav, R. S. Allu, and G. Hua, "High quality image processing system for ADAS," in *Proc. IEEE Int. Conf. Electron., Comput. Commun. Technol. (CONECCT)*, Jul. 2019, pp. 1–4.
- [13] *Laboratory Test Procedure For FMVSS 111 Rear Visibility (Other than School Buses)*. Accessed: Apr. 2021. [Online]. Available: [https://www.nhtsa.gov/sites/nhtsa.gov/files/documents/tp-111-v01-final\\_tag.pdf](https://www.nhtsa.gov/sites/nhtsa.gov/files/documents/tp-111-v01-final_tag.pdf)
- [14] *FMVSS 111 Rear Visibility Full Compliance Requirements: How Commercial Vehicles are Affected*. Accessed: Apr. 2021. [Online]. Available: [https://www.rearviewsafety.com/pub/static/version1558698936/frontend/rearviewsafety/theme/en\\_US/images/FMVSS-111-Full-Compliance.pdf](https://www.rearviewsafety.com/pub/static/version1558698936/frontend/rearviewsafety/theme/en_US/images/FMVSS-111-Full-Compliance.pdf)
- [15] J. Kannala and S. S. Brandt, "A generic camera model and calibration method for conventional, wide-angle, and fish-eye lenses," *IEEE Trans. Pattern Anal. Mach. Intell.*, vol. 28, no. 8, pp. 1335–1340, Aug. 2006.
- [16] E. Schwalbe, "Geometric modelling and calibration of fisheye lens camera systems," in *Proc. 2nd Panoramam Photogramm. Workshop, Int. Arch. Photogramm. Remote Sens.*, 2005, p. W8.
- [17] J. Bergstra and Y. Bengio, "Random search for hyper-parameter optimization," *J. Mach. Learn. Res.*, vol. 13, pp. 281–305, Feb. 2012.



**YOUN JOO LEE** received the B.S. degree in electronic engineering from Konkuk University, Seoul, South Korea, in 2003, and the M.S. and Ph.D. degrees in electrical and electronic engineering from Yonsei University, Seoul, in 2006 and 2013, respectively. From 2013 to 2015, she was with the Biomedical Research Institute, Korea Institute of Science and Technology, Seoul. From 2017 to July 2020, she was with the Korea National University of Transportation, Chungju, South Korea. She is currently a Research Professor with the Next Generation Unmanned Vehicles Research Center, Sejong University, Seoul. Her research interests include computer vision, image analysis, pattern recognition, vehicle localization, and sensor fusion for intelligent vehicles.



**JAЕ KYU SUHR** (Member, IEEE) received the B.S. degree in electronic engineering from Inha University, Incheon, South Korea, in 2005, and the M.S. and Ph.D. degrees in electrical and electronic engineering from Yonsei University, Seoul, South Korea, in 2007 and 2011, respectively. From 2011 to 2016, he was with the Automotive Research Center, Hanyang University, Seoul. From 2016 to 2017, he was with the Korea National University of Transportation, Chungju, South Korea. He is currently an Assistant Professor with the School of Intelligent Mechatronics Engineering, Sejong University, Seoul. His research interests include computer vision, image analysis, pattern recognition, and sensor fusion for intelligent vehicles.



**HO GI JUNG** (Senior Member, IEEE) received the B.E., M.E., and Ph.D. degrees in electronic engineering from Yonsei University, Seoul, South Korea, in 1995, 1997, and 2008, respectively. From 1997 to April 2009, he was with MANDO Corporation Global Research and Development Headquarters, where he developed environmental recognition systems for various driver assistant systems. From May 2009 to February 2011, he was a full-time Researcher and a Research Professor with Yonsei University. From March 2011 to July 2016, he was an Assistant Professor with Hanyang University, Seoul. Since August 2016, he has been a Full Professor with the Korea National University of Transportation, Chungju, South Korea. He is also involved in recognition systems for intelligent vehicles. His research interests include recognition systems for intelligent vehicles, next-generation vehicles, computer vision applications, and pattern recognition applications. He is an Associate Editor of the IEEE TRANSACTIONS ON INTELLIGENT TRANSPORTATION SYSTEMS and the IEEE TRANSACTIONS ON INTELLIGENT VEHICLES.

...